# Geophysical-geotechnical sensor networks for slope stability monitoring

JONATHAN E. CHAMBERS[1], PHILIP I. MELDRUM[1], PAUL B. WILKINSON[1], DAVID A. GUNN[1], OLIVER KURAS[1], JOANNA WRAGG[1] and CHRIS MUNRO[1]

[1] British Geological Survey, Keyworth, Nottingham, NG12 5GG.

jecha@bgs.ac.uk

## Abstract

Slopes, such as earth embankments, can be vulnerable to instability triggered by sustained wetting or drying events. The resilience of earth structures to these climatic stresses, particularly in the case of old waterway and railway embankments, can be difficult to determine due to the complexity of fill materials and the limitations of current approaches to characterisation and monitoring. For example, remote observation of change in surface morphology generally indicates late-stage failure, whilst point sensors provide insufficient spatial sampling density to adequately characterise, and therefore monitor, highly heterogeneous subsurface conditions.

Recent developments in geoelectrical imaging technology now enable full 3D characterisation and monitoring of earth structures to reveal compositional and moisture related variability. Here we describe a study in which automated time-lapse electrical resistivity tomography (ALERT) monitoring technology has been installed on a section of Victorian embankment on the Great Central Railway (Nottingham). Through establishing geophysical-geotechnical property relationships by laboratory testing, electrical resistivity tomography (ERT) monitoring has been used to characterise the internal structure of the embankment, and image moisture content changes and wetting front development at a high spatial resolution. These preliminary results indicate that ERT has the potential to identify structures and processes related to instability at an early stage in their development.

## Introduction

Here we investigate the use of ERT for monitoring moisture content changes in an engineered earth structure. We consider methodologies for correcting ERT models for the effects of seasonal temperature changes, and the translation of resistivity into moisture content using laboratory derived resistivity-moisture content relationships. The resulting images show the spatial distribution of moisture content, which when considered alongside other geotechnical properties, including liquid and plastic limits, provide a basis for predicting the likely changes in stability associated with wetting and drying cycles within the embankment material.


**Fig. 1**: Location map showing the Great Central Railway, and the location of the test site.

## Site Description

The study site is located on a section of Victorian Great Central Railway embankment between Nottingham and Loughborough (Figure 1), which is currently used as a freight and heritage line. The embankment runs approximately north-south, and is located on a natural slope dipping a few degrees towards the west. In the area of the study site the embankment is approximately 5.5 m high and 30 m wide, and is constructed from end-tipped Westbury Formation Mudstone, sourced from a cutting situated less than 1 km to the south. Investigations at the site have demonstrated that the embankment is highly heterogeneous, due to the end-tipping technique used in its construction, comprising re-worked mudstone gravel of angular lithoclasts of the Westbury Formation with sporadic cobbles of Blue Anchor Formation (GUNN et al., 2009). The embankment rests on Branscombe Formation Mudstone Bedrock.

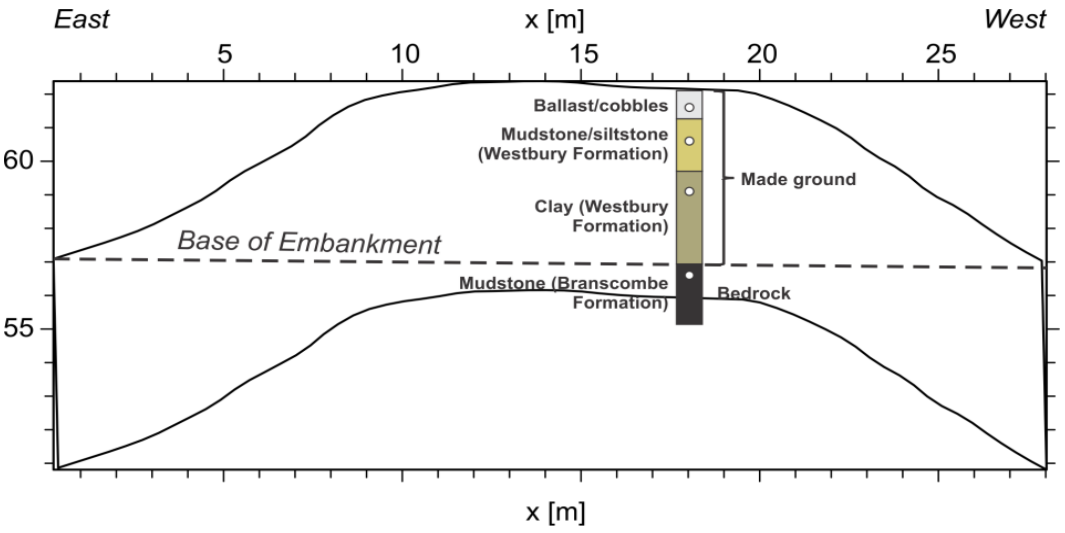


**Fig. 2**: Cross-section through the embankment at *y* = 12 m, showing topography, borehole log, depth to bedrock (dashed line), and temperature sensor locations (white circles).

## Methodology

ERT Monitoring

Permanent ERT Monitoring arrays have been installed within a 22 m section of the embankment as a series of twelve lines at 2 m intervals running perpendicular to the rails. Each line comprised 32 electrodes at 1 m intervals, running from the toe of the eastern flank to the toe of the western flank. Initial 2D ERT measurements, which commenced during July 2006, were made on 2D arrays using a Super Sting R8/IP resistivity instrument during visits to the site. During August 2010 a semi-permanent resistivity system (ALERT, Figure 3; OGILVY et al., 2009) was installed along with additional 3D imaging arrays for automated remote monitoring of the embankment, thereby eliminating the need for repeat monitoring visits to the site and enabling significantly improved temporal resolution (i.e. a measurement frequency of hours as compared to weeks). The 2D imaging line ($y$ = 12 m, $x$ = 0 to 31m) is located within the 3D imaging area ($y$ = 0 to 22 m, $x$ = 0 to 31 m). The $y$-axis is parallel to the rails.

All resistivity data were collected using the dipole-dipole array configuration, with dipole sizes ($a$) of 1, 2, 3 and 4 m, and unit dipole separations ($n$) of 1 to 8. The dipole-dipole command sequences comprised full sets of both normal and reciprocal configurations; comparison of forward and reciprocal measurements provided a robust means of assessing data quality and determining reliable and quantitative data editing criteria.

The 2D and 3D ERT data were inverted using the regularized least-squares optimization method (LOKE and BARKER, 1995, 1996), in which the forward problem was solved using the finite difference method. Sequential time-lapse inversion of the 2D ERT data was carried out using the approach described by CHAMBERS et al. (2010). Good convergence between the observed and model data was achieved for both the 2D and the 3D models, as indicated by RMS errors of between 2.5 and 4.1%, and 6.9% respectively.

**Fig. 3:** Installation of ALERT monitoring instrumentation at the GCR(N) test site.

Temperature Modelling and Resistivity Model Corrections

Monitoring using multi-level sensors (Figure 2) has been undertaken at the test site to determine seasonal temperature changes in the subsurface (Figure 4); these data have been used to correct the time-lapse ERT images for temperature effects using a methodology similar to that described

by BRUNET et al. (2010). Seasonal temperature changes in the subsurface can be described by the following equation,

$$T(z,t) = T_{\text{mean}}(air) + \frac{A}{2} e^{-(z/d)} \sin\left(\omega t + \varphi - z/d\right) \qquad \text{Equation 1}$$

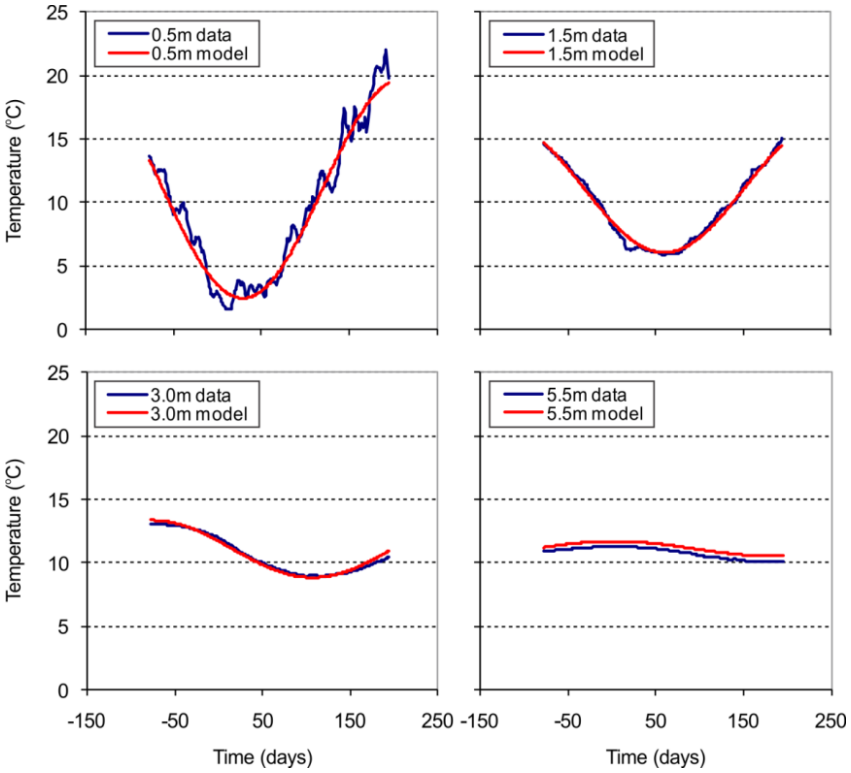


**Fig. 4:** Observed (October 2009-July 2010) & modelled ground temperatures, Great Central Railway test site.

where $T(z,t)$ is the temperature at day $t$ and depth $z$, $T_{\text{mean}}$(air) is the mean yearly air temperature, $A$ is the yearly amplitude of the air temperature variation, $d$ is the characteristic penetration depth of the temperature variation, $\varphi$ is the phase offset, $(\phi - z/d)$ is the phase lag, and ω is the angular frequency ($2\pi/365$). We fitted the temperature data (Figure 4) to Equation 1 using the FindMinimum[] function in the Mathematica computational algebra package. This is a Quasi-Newton method, which uses the Broyden–Fletcher–Goldfarb–Shanno algorithm to update the approximated Hessian matrix (PRESS et al. 1992). The modelled seasonal temperature variations with depth were used to correct the 2D and 3D ERT models, with the assumption that resistivity decreases by 2% per 1 degree C increase in temperature (HAYLEY et al., 2007). Resistivities for all ERT models were normalised to the mean air temperature (11.1°C).

Resistivity-Moisture Content Relationship

Laboratory measurements have been carried out to establish the relationship between resistivity and gravimetric moisture content in the material used to construct the embankment within the area of the study site. Core samples were gathered via drilling sorties in September 2005 and July 2006. The core was sub-sampled into 200 mm sections, which were used to determine a range of estimated values of porosity, density and moisture content for the fill and bedrock.

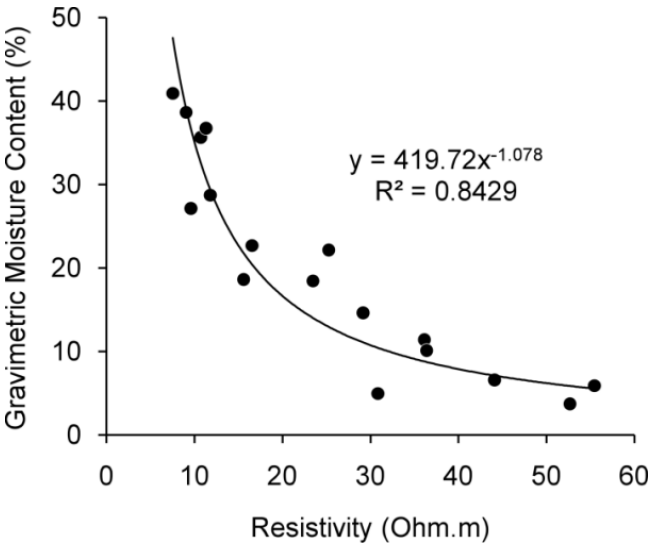


**Fig. 5**: Variation in resistivity with gravimetric moisture content in laboratory samples derived from Westbury Mudstone Formation embankment material taken from the Great Central Railway test site.

Samples were gently crushed to remove particles greater than 8 mm and re-saturated using distilled, deionised water to moisture contents ranging from below the shrinkage limit and up to the liquid limit - in practice this ranges from 5% to 40% w/w. The re-saturated materials were compacted into 100 mm diameter by 100 mm long core liners and sealed with plastic end caps. Sample moisture contents were verified on surplus material during preparation, and the sample masses were measured throughout testing to monitor moisture loss, which was less than 0.1%. Multiple samples of reworked Westbury Formation Mudstone taken from different locations within the study area were used for the tests to reflect the effects of the heterogeneity (e.g., mineralogical and geotechnical property variations) observed in the embankment into the results. Resistivity measurements were made using a non-contact, inductive logging tool (JACKSON et al., 2006). Prior to measurement, all samples were conditioned for at least 24 hours at a constant temperature in a temperature controlled cabinet. The electrical conductivity logging equipment was also conditioned at the same temperature, as were three additional fluid calibration samples of the same dimensions and of known resistivities 20, 200 and 2000 Ωm. At each selected measurement temperature, the internal temperature of a further water filled sample was used as a proxy to monitor any change in temperature within the test samples during the measurement phases. The temperature of the measuring head of the logger was also monitored to gauge the effect upon the test results. The relationship between resistivity and gravimetric moisture content is given in Figure 5.

## Results

Temperature-corrected 2D resistivity and log resistivity ratio plots are shown in Figure 6 for a monitoring period between October 2009 and July 2010, which captures a complete seasonal wetting and drying cycle. ERT derived 2D moisture content and moisture content ratio plots for the same period are shown in Figure 7, and rainfall and air temperature records are shown in Figure 8. 3D baseline resistivity and moisture content images from September 2010 are shown in Figure 9. The 2D results are located on a vertical section located at *y* = 12 m relative to the 3D imaging area (Figure 9).

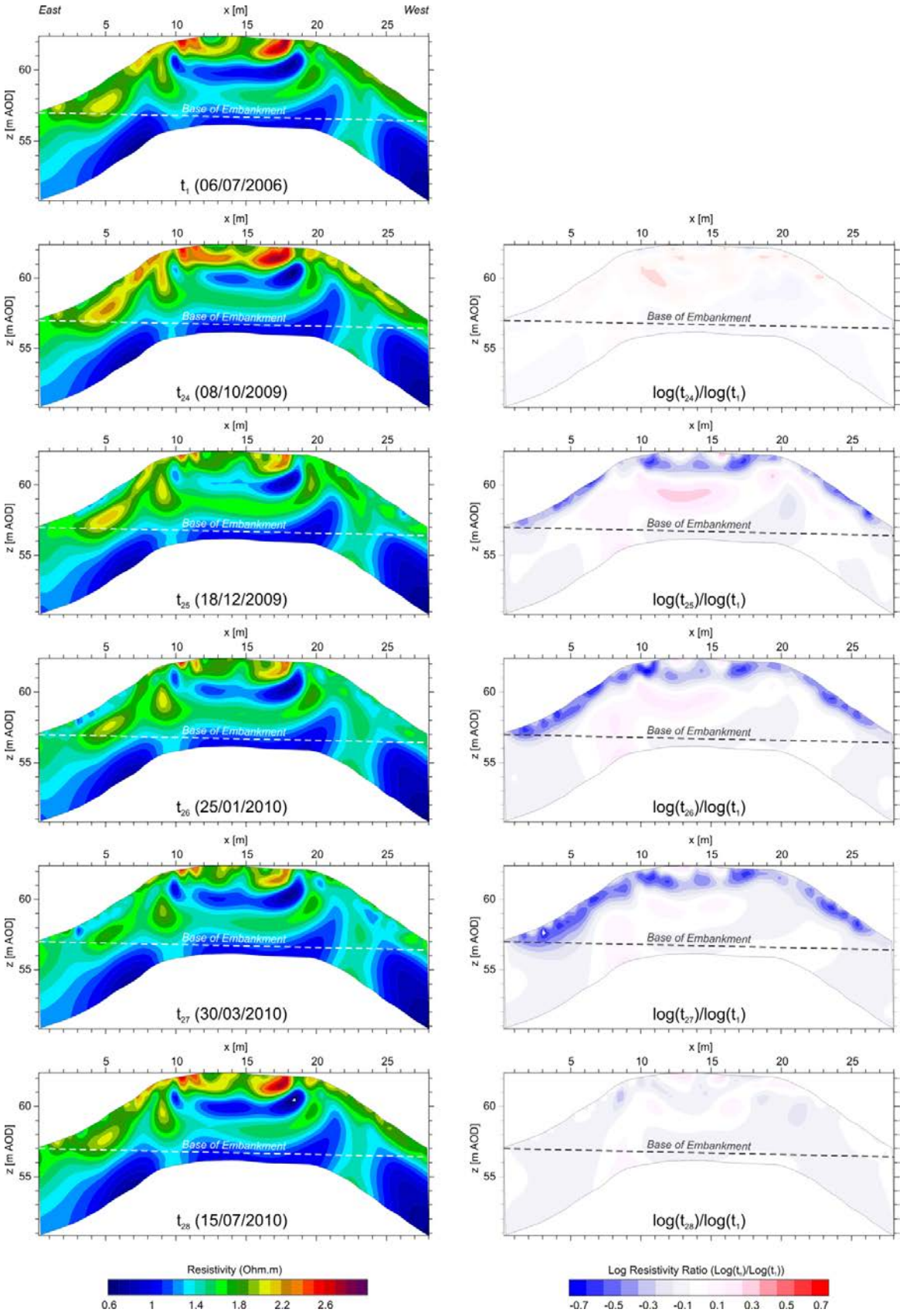


**Fig. 6**: Temperature corrected 2D ERT model sections (left) and log resistivity ratio plots (right) showing changes in resistivity relative to the July 2006 baseline (top left).

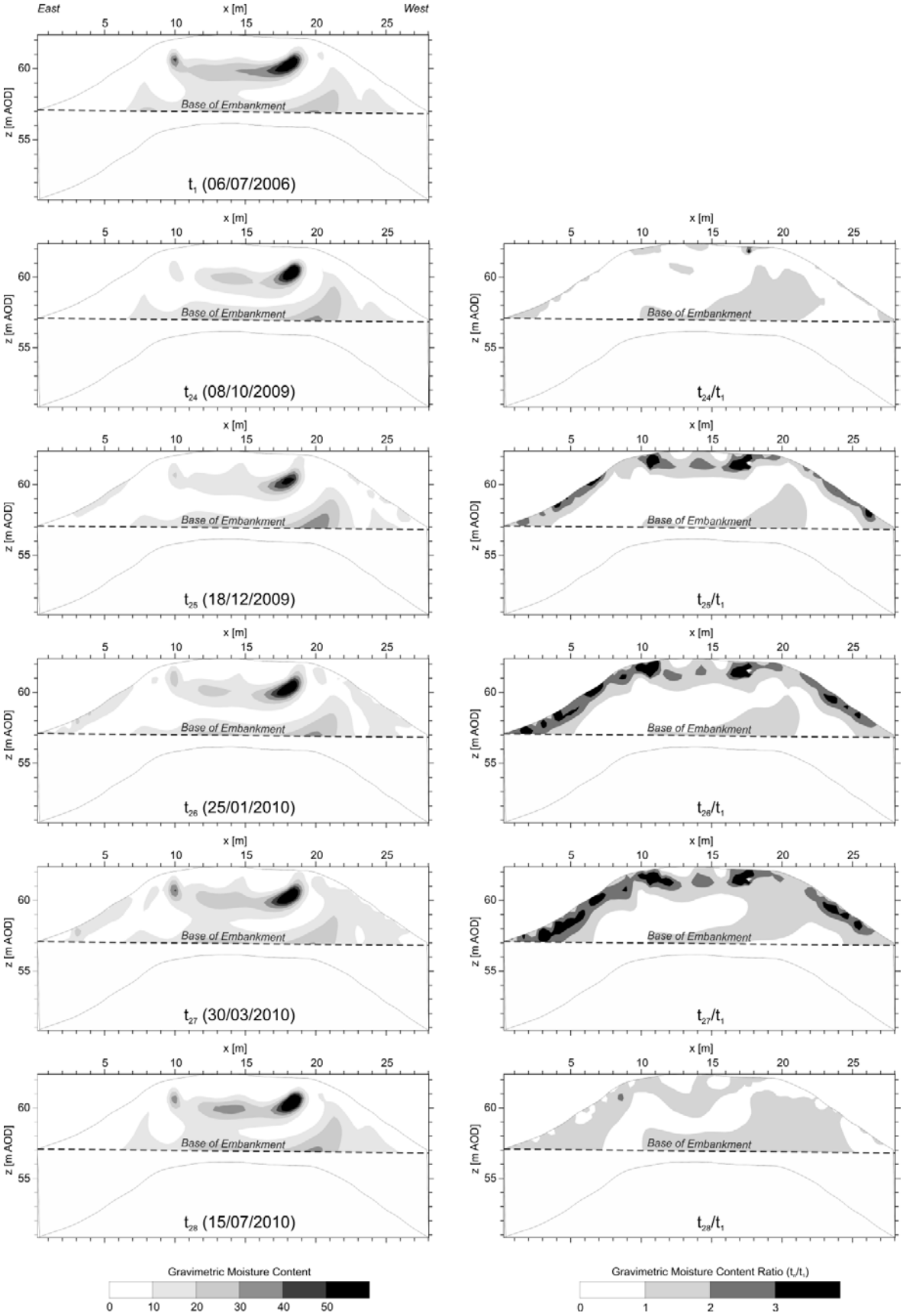


**Fig. 7:** ERT derived gravimetric moisture content (left) and ratio (right) plots calculated using the resistivity moisture content relationships determined from laboratory testing (Figure 5).

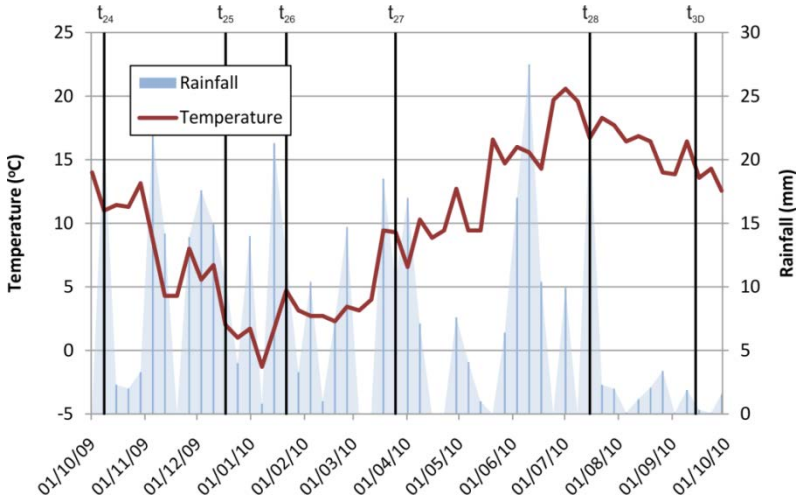


**Fig. 8:** Weekly rainfall and mean air temperature records (~8 km from the test site).

2D Time-lapse Imaging

The resistivity model sections display significant heterogeneity, consistent with the findings of intrusive sampling at the site (e.g. GUNN et al., 2009). In particular, a layered structure in the core of the embankment, and a temporally and spatially varying layer (~ 2 m thick) across the flanks and crest are apparent in the models. The internal layered structure is likely to be a function of both compositional and moisture content variations. Intrusive investigations in the form of borehole (Figure 2) and friction ratio logs (GUNN et al., 2009) indicate a ~ 2 m layer of granular material at the surface overlying more clayey fill, which is likely to account for the more resistive material on the crest. Lower resistivities at the base of the embankment may be related to elevated moisture contents resulting from water draining down slope from the east and perching on the bedrock.

The effects of temporal variations in moisture content are indicated in the log resistivity ratio plots, which show that changes are concentrated predominantly in the upper 2 m of the flanks and crest. These changes show the development of a wetting front during the winter months (indicated by a decrease in resistivity) associated with higher rainfall, lower temperature (Figure 8) and lower evapotranspiration.

The ERT derived gravimetric moisture content and moisture content ratio plots (Figure 7) have been masked below bedrock level. This is because the laboratory derived resistivity-moisture relationships used in the property translation are valid for Westbury Formation Mudstone embankment material, and not the Branscombe Formation Mudstone bedrock. The moisture content sections indicate that moisture levels are generally significantly below the liquid limit of the Westbury Mudstone Formation. The wettest zone (30-40%) is in the core of the embankment within a layer between ~2 and 4 m below the crest. This zone persists throughout the summer and winter months, and is located in the clayey fill materials, which may retain moisture more effectively than the more granular overlying materials.

Moisture contents associated with seasonal variations on the flanks and crest are relatively low (<20%), indicating that significant instability on the flanks or crest is unlikely even during the wettest periods of the year.

Volumetric (3D) Imaging

Baseline volumetric resistivity and moisture content images (Figure 9) reveal significant heterogeneity in the embankment. In the case of the moisture content image, the relatively wet core and dry flanks of the embankment are clearly shown. Ongoing monitoring efforts at the site are now focussing on automated remote monitoring and the collection of volumetric (4D) images.

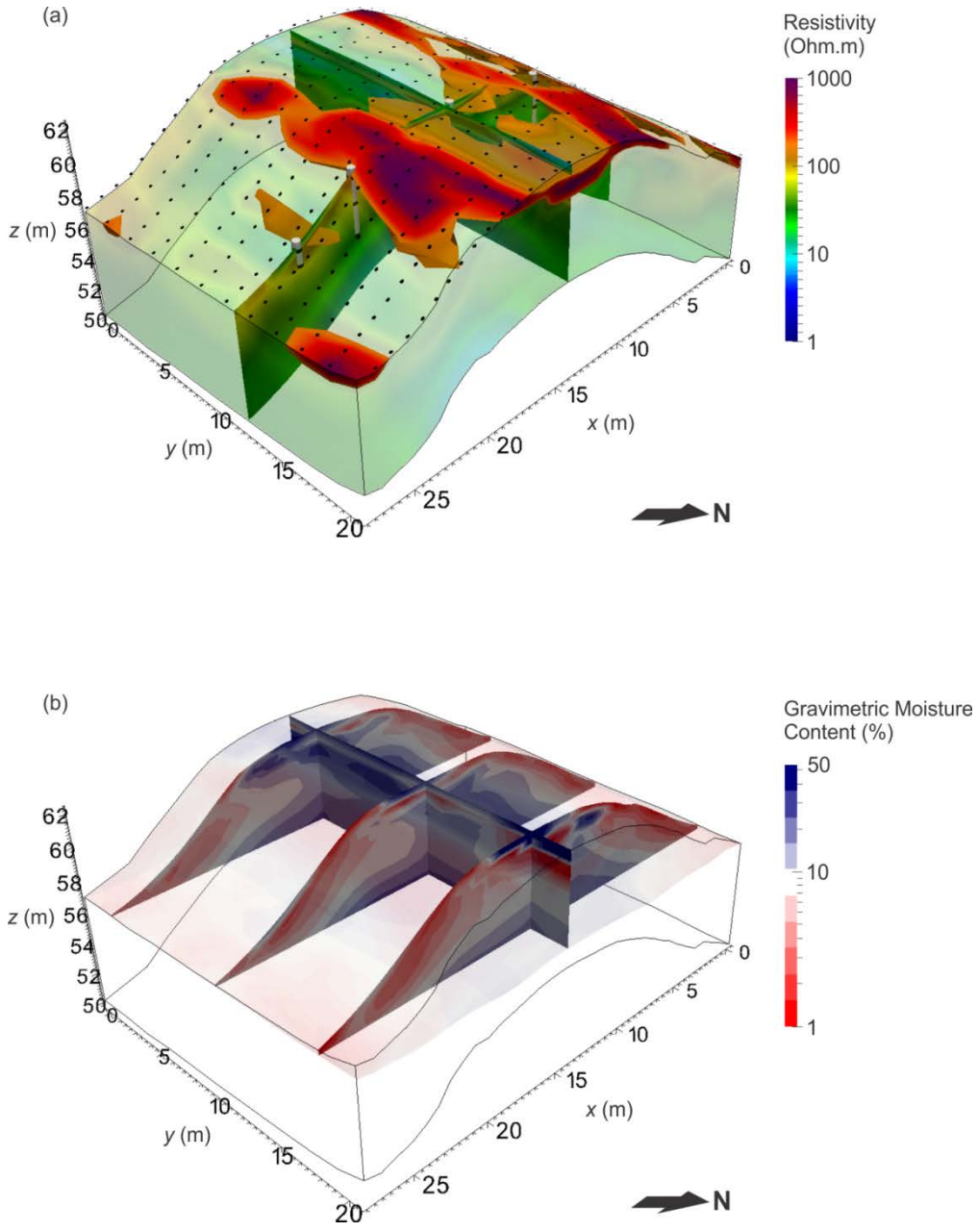


**Fig. 9:** Volumetric images of (a) resistivity and (b) ERT derived gravimetric moisture content, September 2010.

## Conclusions

The use of 2D and 3D ERT as a means of estimating moisture content changes within an earth railway embankment has been demonstrated. A workflow has been described that incorporates the correction of resistivity models for seasonal temperature changes, and the translation of subsurface resistivity distributions into moisture content. Although the moisture content ranges

observed at this site are not a cause for concern, the methodology demonstrated here is applicable to other more vulnerable engineered earth structures and natural slopes. The results clearly demonstrate the potential of ALERT technology for the remote, real-time condition monitoring of slopes.

## Acknowledgements

This paper is published with the permission of the Executive Director of the British Geological Survey (NERC). We also gratefully acknowledge the Great Central Railway (Nottingham) Ltd. for allowing access on to the East Leake embankment. This research has been supported by the East Midlands Development Agency (emda) via the Single Programme fund.

## References

BRUNET, P., CLEMENT, R. and BOUVIER, C., 2010: Monitoring soil water content and deficit using Electrical Resistivity Tomography (ERT) – A case study in the Cevennes area, France. – Journal of Hydrology, **380**, 146-153.

CHAMBERS, J.E., WILKINSON, P.B., WEALTHALL, G.P., LOKE, M.H., DEARDEN, R., WILSON, R., ALLEN, D. and OGILVY, R.D., 2010: Hydrogeophysical imaging of deposit heterogeneity and groundwater chemistry changes during DNAPL source zone bioremediation. – Journal of Contaminant Hydrology, **118**, 43-61.

GUNN, D.A., HASLAM, E., KIRKHAM, M., CHAMBERS, J.E., LACINSKA, A., MILODOWSKI, A., REEVES, H., GHATAORA, G., BURROW, M., WESTON, P., THOMAS, A., DIXON, N., SELLERS, R. and DIJKSTRA, T., 2009: Moisture measurements in an end-tipped embankment: Application for studying long term stability and ageing. – Proc. 10th Int. Conf. Railway Engineering, London.

HAYLEY, K., BENTLEY, L.R., GHARIBI, M. and NIGHTINGALE, M., 2007: Low temperature dependence of electrical resistivity: Implications for near surface geophysical monitoring. – Geophysical Research Letters, **34**, L18402.

JACKSON, P.D., LOVELL, M.A., ROBERTS, J.A., SCHULTHEISS, P.J., GUNN, D., FLINT, R.C., WOOD, A., HOLMES, R. and FREDERICHS, T., 2006: Rapid non-contacting resistivity logging of core. – In: ROTHWELL, R.G. (Ed.): New techniques in sediment core analysis. – Geological Society Special Publication SP **267**.

LOKE, M.H. and BARKER, R.D., 1995: Least-Squares Deconvolution of Apparent Resistivity Pseudosections. – Geophysics, **60**, 1682-1690.

LOKE, M.H. and BARKER, R.D., 1996: Practical techniques for 3D resistivity surveys and data inversion. – Geophysical Prospecting, **44**(3), 499-523.

OGILVY, R.D., MELDRUM, P.I., KURAS, O., WILKINSON, P.B., CHAMBERS, J.E., SEN, M., PULIDO-BOSCH, A., GISBERT, J., JORRETO, S., FRANCES, I. and TSOURLOS, P., 2009: Automated monitoring of coastal aquifers with electrical resistivity tomography. – Near Surface Geophysics, **7**, 367-375.

PRESS, W.H., TEUKOLSKY, S.A., VETTERLING, W.T. and FLANNERY, B.P., 1992: Numerical Recipes in C: The Art of Scientific Computing, 2nd edition, Cambridge University Press, Cambridge.